Applied Catalysis B: Environmental 185 (2016) 100–109

Contents lists available at ScienceDirect

Applied Catalysis B: Environmental

journal homepage: www.elsevier.com/locate/apcatb

Selective *p*-xylene production from biomass-derived dimethylfuran and ethylene over zeolite beta nanosponge catalysts

Tae-Wan Kim[a,*], Sang-Yun Kim[a], Jeong-Chul Kim[b,c], Youngjin Kim[b,d], Ryong Ryoo[b,e], Chul-Ung Kim[a,*]

[a] Research Center for Carbon Resource Conversion, Korea Research Institute of Chemical Technology, 141 Gajeong-ro, Yuseong-gu, Daejeon 305-600, Republic of Korea
[b] Center for Nanomaterials and Chemical Reactions, Institute for Basic Science (IBS), Daejeon 305-701, Republic of Korea
[c] Graduate School of Nanoscience and Technology, KAIST, Daejeon 305-701, Republic of Korea
[d] Department of Chemical and Biomolecular Engineering, KAIST, Daejeon 305-701, Republic of Korea
[e] Department of Chemistry, KAIST, Daejeon 305-701, Republic of Korea

ARTICLE INFO

Article history:
Received 9 September 2015
Received in revised form
11 November 2015
Accepted 23 November 2015
Available online 3 December 2015

Keywords:
p-Xylene
Mesoporous zeolite
Cycloaddition
Dimethylfuran
Beta zeolite

ABSTRACT

p-Xylene can be synthesized via a renewable route from biomass-derived 2,5-dimethylfuran (DMF) and ethylene with zeolite catalysts. Here, we propose mesoporous beta zeolite with a nanosponge-like morphology (NSP-BEA) as a highly efficient catalyst for the cycloaddition of DMF with ethylene. The NSP-BEA zeolite was synthesized through a hydrothermal synthesis route using multi-ammonium surfactants as a meso–micro dual structure-directing agent. From structural analyses and measurements of the surface acidity, the NSP-BEA was found to be composed of ultrathin zeolitic nanocrystals with intercrystalline mesopores (~4.5 nm). It also possessed a large number of Brønsted acid sites on its external surfaces and in its internal micropores. This NSP-BEA catalyst exhibited high catalytic performance upon a cycloaddition of DMF with ethylene as compared to the commercial beta zeolite, alumina, and silica–alumina catalysts reported previously.

1. Introduction

p-Xylene (PX), an important large-volume commodity chemical in the petrochemical industry, is mainly used to produce terephthalic acid (TPA) [1,2], which is the co-monomer in a condensation with monoethylene glycol (MEG) for the manufacturing of polyethylene terephthalate (PET) [2,3]. Over 50 million tons of PET are globally produced per year [4], and PET is widely used in common applications to create plastics, films, and synthetic fibers. Due to the continuous growth of the global economy, the global PET market is also expected to grow by approximately 8% per year consistently [5–7]. Such large growth of the global PET market makes PX an important chemical as well as a key target with regard to the development of new technologies using renewable resources due to current situations such as the continuing unstable oil price, the depletion of petroleum, efforts to reduce greenhouse gas emissions, and the increasing requirement of the use of renewable feedstocks [2,4,8–10].

At present, the dominant technology for the production of PX is the petroleum-derived naphtha cracking process, where PX is obtained as a co-product. However, PX should be separated from mixtures of aromatics such as benzene and toluene as well as *o*-, *m*-, and *p*-xylenes because the production of PET requires high-purity PX. Thus, to purify PX, the aromatic mixture is treated with several separation technologies such as distillation, crystallization, and adsorption [11–13]. In contrast, the naphtha cracking process, a catalytically direct and selective PX production process involving the use of petroleum-based feedstock, remains not fully developed. The catalytic production of PX from petroleum-derived toluene has been reported by several researchers [14–20]. However, long-term shortages of aromatic chemicals are expected to results from the availability of the considerable quantities of natural gas caused by the recent American shale-gas revolution. Natural gas is going to displace naphtha as a primary feedstock in the petrochemical industry, which has motivated a push toward the development of alternative technologies for PX production from renewable, and non-petroleum resources [2,4,9,10,21].

Recently, companies and researchers have proposed an alternative route for the production of PX from renewable feedstocks. Virent developed a technology which converts C_5/C_6 sugars to

* Corresponding author. Fax: +82 42 860 7508.
E-mail addresses: twkim@krict.re.kr (T.-W. Kim), cukim@krict.re.kr (C.-U. Kim).

http://dx.doi.org/10.1016/j.apcatb.2015.11.046
0926-3373/

a mixture of benzene, toluene, and xylenes (BTX) by means of aqueous-phase reforming and dehydrocyclization (BioForming® process) [22,23]. The resultant aromatic mixtures can serve as a drop-in feedstock in typical PX separation/purification processes, but the high cost of mixed xylene purification is not avoided. Anellotech and Prof. George W. Huber developed catalytic fast pyrolysis technology for the production of a drop-in BTX stream from lignocellulosic biomass in a single reaction. Biomass is rapidly heated under an anaerobic condition, and the resulting gases immediately are converted to aromatics by a zeolite catalyst [24,25]. In addition to producing a drop-in BTX mixture from renewable sources, Gevo developed a process which directly produces PX from isobutanol without a separation process. They produce isobutanol from starch and cellulose through a fermentation process in the presence of a microorganism which they developed. The isobutanol can be finally converted to PX via a series of chemical processes (dehydration, oligomerization, and dehydrocyclization) [26,27]. However, this technology involves complicated reaction processes and results in a low product yield during the fermentation process. It also consumes a considerable amount of energy during the removal of a large quantity of water.

The other potential route for the direct and selective production of bio-based PX is the Diels–Alder (DA) cycloaddition of biomass-derived 2,5-dimethylfuran (DMF) and ethylene followed by the dehydration of an intermediate (Scheme 1) [28–33]. This process is based on the concept of the production of 5-hydroxymethylfurfural (HMF) from cellulose as a raw material. HMF is one of the most promising biomass-derived intermediates [34], and it can be converted to DMF via hydrogenolysis with a high yield [35]. UOP has patented the catalytic conversion process of DMF to PX via the DA cycloaddition of ethylene to DMF using activated carbon, zeolites, and other porous solids [29]. The PX yield for the best-performing activated carbon catalyst in a batch reactor is as high as 78% of the total weight of all converted materials, and the one-pass conversion of DMF to PX is approximately 30% in a continuous fixed-bed reactor. Toray has also disclosed a PX production process via a DA cycloaddition reaction of DMF with ethylene using a composite oxide containing a silica-alumina in a patent [33]. Silica-alumina with titanium metal salt is used as a DA catalyst, and the PX yield is 96 wt% of the remaining organic materials in the reaction ampoule. Recently, researchers at the University of Massachusetts Amherst and at the University of Delaware reported the catalytic conversion of DMF and ethylene to PX with good selectivity through a combination of DA cycloaddition and dehydration reactions over zeolite catalysts [28]. They achieved PX selectivity of approximately 75% and DMF conversion of nearly 95% with H-Y zeolite using *n*-heptane as a solvent in a batch reactor. The DA cycloaddition of DMF and ethylene is promoted by confinement within the uniform micropores of zeolite catalysts. They also suggested possible reaction pathways and energetics of the reaction via the identification of the reaction products, and through a DFT study [30,31]. Wang et al. demonstrated that the acidic solid catalyst WO_x-ZrO_2 shows significant PX production via the DA cycloaddition of DMF and ethylene [36]. They concluded that Brønsted acid sites in the solid acid catalyst are active for PX production, with microporosity of the zeolite catalysts not required. More recently, the same group at the university of Massachusetts Amherst achieved PX selectivity and yields which both exceeded 90% in a DA cycloaddition reaction of DMF and ethylene with H-BEA zeolite in *n*-heptane [32]. H-BEA zeolite was assumed to suppress side reactions, which results in superior activity of H-BEA relative to those of other solid acids.

Despite showing excellent catalytic activity with good PX selectivity, H-BEA zeolite would show insufficient activity with fast catalytic deactivation, which is similar to other reactions using zeolitic microporous catalysts due to coke formation in the micropores. From the GC–MS and 2D-NMR analytic techniques, the DA reaction of DMF and ethylene using a zeolite catalyst produces many bulky byproducts such as dimers, oligomers, and alkylated aromatics [31]. These bulky byproducts would be trapped in the small channels of the zeolite catalyst, leading to coke formation in the micropores, after which the zeolite catalyst would be deactivated. Moreover, the microporous properties of the zeolite materials cause significant pore resistance for the transportation of a liquid-phase reactant (DMF) to the catalytic active sites. The pore resistance may also affect the catalytic activity in this reactions. Therefore, it is very important to investigate the structural properties of zeolite catalyst that can reduce catalytic deactivation by means of coke formation and pore resistance.

In 2011, Ryoo and co-workers reported the direct synthesis of a hierarchically mesoporous zeolite using multi-ammonium surfactants as a meso–micro dual-structure-directing agent (SDA) [37–45]. Multi-ammonium surfactants are specially designed in a combination of cationic moieties and long alkyl chains for the formation of a microporous zeolitic framework (e.g., MFI, MTW, MRE, and Beta) and a hexagonally ordered or disordered mesostructure (e.g., nanosheet- or nanosponge-like morphologies), respectively. Typically, beta zeolite with a nanosponge-like morphology (NSP-BEA in short) was synthesized using [$C_{22}H_{45}$-$N^+(CH_3)_2$-C_6H_{12}-$N^+(CH_3)_2$-CH_2-(C_6H_4)-CH_2-$N^+(CH_3)_2$-C_6H_{12}-$N^+(CH_3)_2$-CH_2-(C_6H_4)-CH_2-$N^+(CH_3)_2$-C_6H_{12}-$N^+(CH_3)_2$-$C_{22}H_{45}(Br^-)_2(Cl^-)_4$]. The NSP-BEA was assembled in irregular 3D networks of zeolitic nanocrystals to possess the intercrystalline mesopores with uniform diameters (~4.5 nm). This NSP-BEA zeolite exhibited superior catalytic activity and a long lifetime during the acid-catalyzed liquid-phase Friedel-Craft alkylation of benzene with benzyl alcohol [41] and the acylation of bulky aromatic compounds [45] as well as gas-phase benzene isopropylation to cumene reaction [38]. This result was explained in consideration of the large number of strong Brønsted acid sites on the external surfaces and the facile diffusion of molecules through the mesopores. Nevertheless, such effects of the mesostructure of the NSP-BEA zeolite on the catalytic performances have not been applied in liquid-phase DMF to the PX process.

In this regard, we investigated the performance of NSP-BEA as a catalyst during the DA cycloaddition of DMF and ethylene. We performed the DA reaction over NSP-BEA with different SiO_2/Al_2O_3 ratios (30 and 50) under various reaction conditions (i.e., various reaction temperatures, pressures, amounts of catalyst, and amounts of DMF in *n*-heptane). These results are discussed in comparison with the catalytic performances of commercial beta zeolite, γ-alumina, and silica-alumina.

2. Experimental

2.1. Preparation of catalysts

The NSP-BEA zeolite was hydrothermally synthesized using [$C_{22}H_{45}$-$N^+(CH_3)_2$-C_6H_{12}-$N^+(CH_3)_2$-CH_2-(C_6H_4)-CH_2-$N^+(CH_3)_2$-C_6H_{12}-$N^+(CH_3)_2$-CH_2-(C_6H_4)-CH_2-$N^+(CH_3)_2$-C_6H_{12}-$N^+(CH_3)_2$-$C_{22}H_{45}(Br^-)_2(Cl^-)_4$] (in short, "$C_{22}$-6N") as a SDA, as described in the literature [41]. In brief, tetraethylorthosilicate (TEOS, 95%, Junsei) was added to a NaOH solution containing both sodium aluminate (53 wt%, Sigma–Aldrich) and C_{22}-6N. The synthesis gel had a composition of 30 SiO_2: *a* Al_2O_3: 1 C_{22}-6N: 6.66 Na_2O: 1500 H_2O, where *a* = 0.6 and 1.0. The mixture was stirred at 60 °C for 6 h, and then heated for 3 days at 140 °C in a Teflon-lined autoclave, for zeolite crystallization. The zeolite products were collected after filtration, washing with water, and dried at 100 °C for 12 h. The obtained zeolites were calcined at 580 °C in air. The zeolite was then ion-exchanged three times with a 1 M NH_4NO_3 solution and subsequently calcined again at 580 °C for its full conversion to the

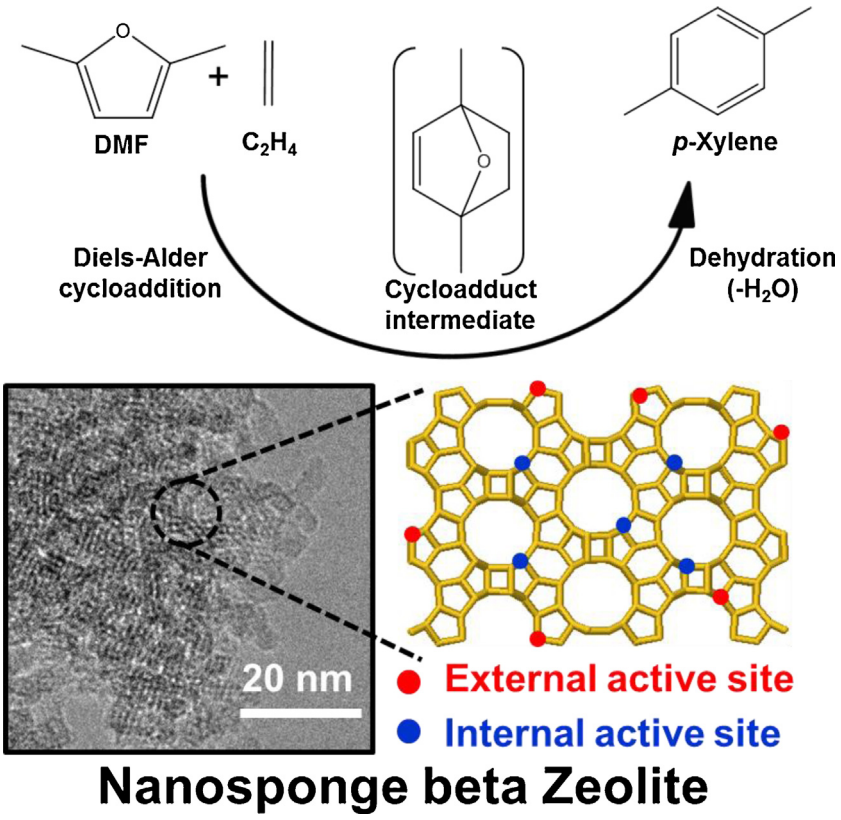

Scheme 1. Schematic illustration for production of PX from DMF with ethylene over NSP-BEA zeolite.

H^+ form. The zeolite sample is denoted as "NSP-BEA (*X*)" according to the SiO_2/Al_2O_3 ratios (*X* = 30 and 50) in the text. For comparison, a commercial beta zeolite in the NH_4^+ form was purchased from Zeolyst (CBV814E, SiO_2/Al_2O_3 = 25) and calcined at 550 °C before use. This sample is designated as "C-BEA" in the text. γ-alumina and silica-alumina were supplied from Stream Chemicals and Sasol (Siral40), and are denoted "γ-Al_2O_3" and "Si–Al–O", respectively.

2.2. Characterization

Powder X-ray diffraction (XRD) patterns were recorded on a Rigaku Multiplex diffractometer equipped with a Cu-Kα radiation operated at 30 kV and 40 mA (1.6 kW). Nitrogen adsorption isotherms were measured at −196 °C with a Micromeritics Tristar II instrument. Before the adsorption measurements, all samples were outgassed at 300 °C for 6 h in a degassing station. The Brunauer–Emmett–Teller (BET) equation was used to calculate the apparent surface area from the adsorption data obtained at a P/P_0 ratio between 0.05 and 0.2. The total volume of the micro- and mesopores was calculated from the amount of nitrogen adsorbed at P/P_0 = 0.95, assuming that adsorption on the external surface was negligible compared to adsorption in the pores. The pore size distributions were calculated by analyzing the adsorption branch of the nitrogen sorption isotherm using the Barret–Joyner–Halenda (BJH) method. Scanning electron micrograph (SEM) images were obtained with a Hitachi S-4800 microscope operating at 2 kV without a metal coating. Transmission electron micrographs (TEM) images were obtained using a TecnaiG2 F30 at an operating voltage of 300 kV. The SiO_2/Al_2O_3 ratios were determined by inductively coupled plasma-atomic emission spectroscopy (ICP-AES) using an OPTIMA 4300 DV instrument (PerkinElmer). The total number of acid sites was measured by the temperature-programmed desorption of ammonia using a BELCAT-M (BEL Japan) instrument equipped with a thermal conductivity detector (TCD). The concentration and location of the Brønsted acidic properties were analyzed using ^{31}P NMR after adsorbing phosphine oxides as probe molecules [39,46]. ^{31}P NMR spectra were acquired in a solid state via magic angle spinning using a Bruker AVANCE400WB spectrometer at room temperature, following a method reported in the literature [39]. Trimethylphosphine oxide was used to detect "the total number of Brønsted acid sites" existing on the internal pore walls and external surfaces of the zeolite crystals. Triphenylphosphine oxide was used to measure the Brønsted acid sites located on the external surfaces of the samples. Coke depositions of the catalyst were investigated by recording weight changes on a thermogravimetric analyzer (TGA Q500, TA Instrument). Runs under air were carried out at a heating rate of 10.0 °C/min to 900 °C.

2.3. Catalytic test

The production of PX from DMF and ethylene was performed in a 250 ml, high-pressure Parr-type reactor system as shown in Fig. S1. Typically, 25 ml of DMF (Acros, 99%) and 75 ml of *n*-heptane (J.T. Baker, 99%) were placed in a batch reactor with 0.2 g of catalyst. The reaction vessel was purged by nitrogen gas and pressurized up to 50 bar for a leak test. After the 24 h leak test, the ethylene gas (99.5%) was purged into the batch reactor three times, and the gas inlet line was then left open during the reaction to ensure a constant ethylene gas supply with a mass flow controller at 50 bar. The reaction was performed at 250 °C with 500 rpm of stirring for 24 h. Liquid samples were taken by a double block sampling system at the desired reaction times. For the catalytic tests done to investigate the reaction conditions of the temperature, pressure, catalyst amount, and DMF/solvent ratio, liquid products were obtained at 24 h. The reaction products were analyzed by a gas chromatography (GC, Acme-6100, Young Lin Instrument Co.) equipped with a

flame ionization detector (FID). Products were identified with the FID using a capillary HP-INNOWAX column (0.32 mm id × 0.5 μm thickness × 60 m length). Fig. S2 shows GC chromatograms of the feed and liquid products before and after the reaction. The conversion of DMF, the selectivities, and the yields of products were calculated by the following equations:

$$\mathrm{Conv}_{\cdot\mathrm{DMF}}(\%) = \frac{(\mathrm{M}_{\mathrm{DMF},t0} - \mathrm{M}_{\mathrm{DMF}})}{\mathrm{M}_{\mathrm{DMF},t0}} \times 100\,\mathrm{Selec}_{\cdot i}(\%)$$

$$= \frac{\mathrm{M}_i}{\Sigma_i \mathrm{M}_i} \times 100\mathrm{Yield}_i(\%) = \frac{\mathrm{Conv}_{\cdot\mathrm{DMF}}\mathrm{x} \times \mathrm{Selec}_{\cdot i}}{100}$$

where, $\mathrm{Conv}._{\mathrm{DMF}}$ denotes conversion of DMF; $\mathrm{M}_{\mathrm{DMF},\,t0}$ represents the mol of DMF at the initial time; $\mathrm{M}_{\mathrm{DMF}}$ is the mol of DMF at the desired reaction time; $\mathrm{Selec}._i$ denotes the selectivity of product i ; M_i is the mol of product i ; Yield_i is yield of product i.

3. Results and discussion

3.1. Properties of NSP-BEA catalysts

Fig. 1(a) shows representative XRD patterns of the C-BEA, γ-Al_2O_3, Si–Al–O, and NSP-BEA samples. The XRD patterns of the C-BEA zeolite exhibited representative Bragg reflections corresponding to the typical beta zeolite structure. The XRD peaks of C-BEA were relatively sharp without a detectable background increase in the 2θ region between 15 and 25° due to the highly crystalline framework. Compared to the C-BEA zeolite, the NSP-BEA zeolite samples with different SiO_2/Al_2O_3 ratios showed two broad peaks (2θ = 7.5° and 22°). These peaks were consistent with the beta zeolite structure [i.e., the (101) and (302) reflections]. The broad peak widths could be attributed to the nano-sized zeolite crystals of the NSP-BEA samples. There were no other distinct reflections due to their low intensities in addition to the peak broadening. For γ-Al_2O_3 and Si–Al–O, the XRD patterns did not show detectable peaks in the 2θ region between 5 and 35° due to the amorphous framework.

Fig. 2 shows representative SEM and TEM images taken of the NSP-BEA and C-BEA samples. Both NSP-BEA samples exhibit a nanosponge-like morphology which is composed of very thin (~5 nm) beta zeolite crystals. These nanocrystals are interconnected to form a 3D disordered network. No amorphous silicate particles, bulk Beta zeolite particles or other impurities were detected in the NSP-BEA samples in the SEM and TEM analyses, in good agreement with the XRD patterns (Fig. 1). On the other hand, the SEM images of the C-BEA zeolite showed the aggregation of beta zeolite crystals with diameters ranging from 50 to 100 nm. The TEM images of C-BEA exhibited a smooth external surface without mesopores as compared to the NSP-BEA zeolites.

The nitrogen adsorption isotherms of the C-BEA, γ-Al_2O_3, Si–Al–O, and NSP-BEA samples at–196 °C are shown in Fig. 1(b). The adsorption isotherms of the NSP-BEA samples exhibit a combination of type- I and IV isotherms with an increase in the adsorbed amount in the medium-pressure region of $0.4 < P/P_0 < 0.5$, as well as a gradual increase in the low-pressure region of $P/P_0 < 0.1$. The first jump can be interpreted as nitrogen filling in the zeolite micropores, while the second increase is attributed to the capillary condensation in the mesopores of the NSP-BEA samples. However, the hysteresis loop of the NSP-BEA samples was different, in the range of $0.4 < P/P_0 < 0.9$. For the NSP-BEA (50) sample, the hysteresis loop has the general H2 form associated with ink-bottle shaped pores. The adsorption isotherm was analyzed using the BJH algorithm, which resulted in a narrow distribution of mesopore diameters that centered at 4.5 nm. For the NSP-BEA (30), the isotherm showed another jump in the high-pressure region of $0.6 < P/P_0 < 1.0$, due to the formation of a secondary mesopore (centered at 25 nm). This large mesopore could be generated as a result of the retaining of pores from the initial gel via a pseudomorphic transformation [47]. Therefore, the NSP-BEA (30) sample (Table S1, 930 m^2/g and 1.4 cm^3/g, respectively) exhibited a much higher specific BET surface area and a larger pore volume than NSP-BEA (50) (820 m^2/g and 0.76 cm^3/g, respectively). Due to the highly mesoporous properties, the NSP-BEA samples exhibited a very high specific area of their external surfaces (650 and 700 m^2/g, respectively). In contrast to the NSP-BEA samples, C-BEA showed solely a microporous structure with a very lower BET surface area, external surface area, and pore volume (460 m^2/g, 50 m^2/g, and 0.24 cm^3/g, respectively).

Table 1 shows the acidic properties of all beta zeolites, γ-Al_2O_3, and Si–Al–O samples. The SiO_2/Al_2O_3 ratios of the NSP-BEA (30) and (50) samples were 31 and 54, respectively, according to an elemental analysis using ICP-AES. The concentrations of the Brønsted acid sites of the NSP-BEA samples were analyzed using solid-state ^{31}P NMR spectroscopy using phosphine oxides as probe molecules. Trimethylphosphine oxide was used for the detection of the total amount of Brønsted acid sites (BA_{tot}). Triphenylphosphine oxide was used to determine the Brønsted acid sites located on the external surfaces (BA_{ext}), as bulky molecules can probe only the external acid sites and cannot enter the micropores. From the results of the ^{31}P NMR measurement, the NSP-BEA samples were found to have Brønsted acid sites (583 and 345 μmol/g, respectively). This result is in good agreement with the Al content of the NSP-BEA samples as confirmed by ICP-AES. Notably, the NSP-BEA samples possessed a large amount of BA_{ext} (194 and 114 μmol/g). The fractions of BA_{ext} were quite high for the NSP-BEA samples (~33%) due to the large external surface area. On the other hand, the C-BEA sample possessed a small amount of BA_{ext} (34 μmol/g, 5% of the total acid sites) as compared with the NSP-BEA samples. Moreover, the Si–Al–O sample had a very small amount of BA_{tot} (66 μmol/g) without external acid sites. For the γ-Al_2O_3 sample, there was no Brønsted acid sites on the catalyst, in good agreement with a previous report [32].

3.2. Catalytic test for PX production from DMF and ethylene over various solid acid catalysts

Fig. 3 shows the reaction rates of the formation of PX from DMF and ethylene with different solid-acid catalysts and with two different initial reaction times (30 min and 1 h) at 250 °C and 50 bar. These reaction rates exhibit the catalytic activities of the catalysts for the formation of PX from DMF and ethylene during the reaction time. With more initial reaction time, 30 min, the order of the PX production rate among these catalysts was C-BEA > NSP-BEA (30) > NSP-BEA (50) > Si–Al–O > γ-Al_2O_3. The C-BEA sample, as previously reported [32], showed the highest PX production rate of more than 200 mmol/(g-cat h). Among the two NSP-BEA zeolites, the catalyst with the low SiO_2/Al_2O_3 ratio [NSP-BEA (30)] exhibited higher catalytic activity than that with the high SiO_2/Al_2O_3 ratio [NSP-BEA (50)]. The γ-Al_2O_3 catalyst demonstrated a very low PX production rate of 4.6 mmol/(g-cat h) compared to other solid-acid catalysts, such as the beta zeolites and Si–Al–O. The lowest catalytic activity in the γ-Al_2O_3 catalyst is due to the surface of the alumina sample, which has only has Lewis acid sites. As shown in Table 1, the γ-Al_2O_3 catalyst does not have Brønsted acid sites, which is essential for the catalytic conversion of DMF and ethylene to PX through a consecutive reaction of DA cycloaddition and dehydration in the solid-acid catalyst. The order of the total number of Brønsted acid sites for these catalysts is C-BEA > NSP-BEA (30) > NSP-BEA (50) > Si–Al–O, which is identical to the order of the PX production rate at 30 min. This clearly indicates that more Brønsted acid sites in solid-acid catalysts leads to higher catalytic activity for the production of PX from DMF and ethylene. A plot of the rate of PX production *versus* the total Brønsted acid sites is

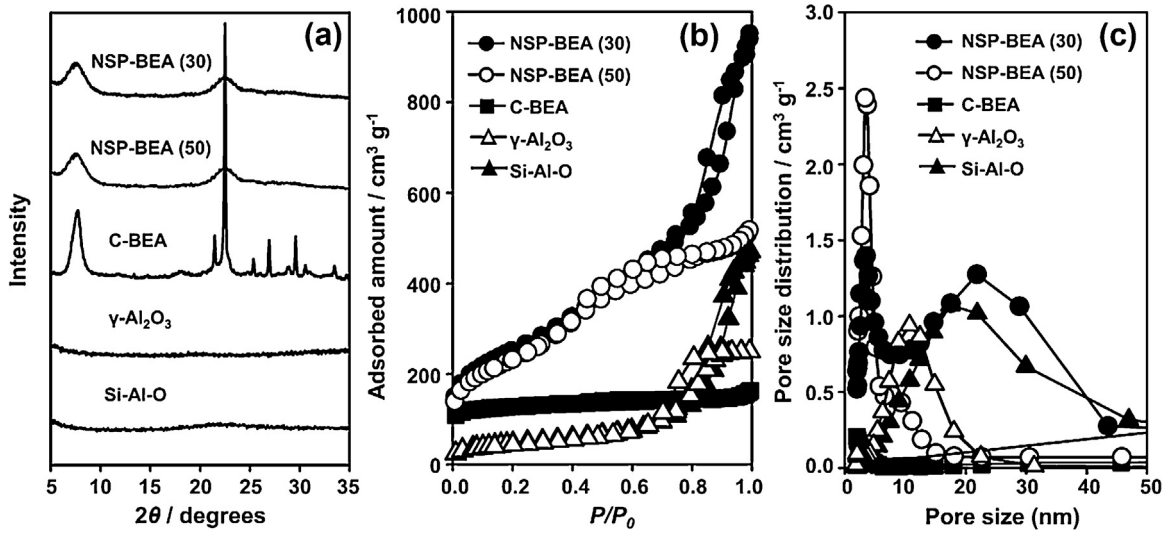

Fig. 1. Powder XRD patterns (a) and nitrogen adsorption isotherms (b) of NSP-BEA (x) (x = 30 and 50), C-BEA, γ-Al_2O_3, Si–Al–O samples. Pore size distributions (c) correspond to the adsorption branch of samples.

Table 1
Physicochemical properties of the NSP-BEA (x) (x = 30 and 50), C-BEA, γ-Al_2O_3, Si–Al–O samples.

Catalyst	SiO_2/Al_2O_3[a]	TA[b] (μmol/g)	BA_{tot}[c] (μmol/g$^-$)	BA_{ext}[d] (μmol/g)	BA_{int}[e] (μmol/g)	H-TOF[f] (10^{-3}/s)
NSP-BEA (30)	31	820	583	194	389	86.3 (84.4)
NSP-BEA (50)	54	480	345	114	231	108.5 (99.5)
C-BEA	26	1144	684	34	650	84.3 (58.1)
γ-Al_2O_3	n.a[g]	609	n.d[h]	n.d	n.d	n.a
Si–Al–O	1	261	66	n.d	n.d	413.4 (385.5)

[a] Si/Al_2 mole ratio obtained from inductively-coupled plasma atomic emission spectroscopy analysis.
[b] TA is the total acidity obtained from NH_3-TPD analysis.
[c] BA_{tot} is the concentration of total Brønsted acid sites.
[d] BA_{ext} is the concentration of external Brønsted acid sites.
[e] BA_{int} is the concentration of internal Brønsted acid sites.
[f] H-TOF is the turnover frequency calculated by normalizing the rate by the number of Brønsted acid sites at the reaction time = 30 min. The values in parentheses are H-TOF at the reaction time = 1 h.
[g] Not applicable.
[h] Not determined.

shown in Fig. 4. The PX production rate as a function of the total number of Brønsted acid sites (BA_{tot}) on the solid-acid catalysts (circle symbols) was found to increase linearly at a reaction time of 30 min, in good agreement with the linear regression curve (solid line).

After 1 h of reaction, the NSP-BEA (30) catalyst exhibited the highest catalytic activity, more active than C-BEA, as shown in Fig. 3 (bottom). The reaction rates of PX formation from DMF and ethylene were slightly decreased in these solid-acid catalysts compared to the reaction rates at a reaction time of 30 min, except for the C-BEA zeolite. The percentages of the decrease in reaction rate were 2.2%, 8.2%, and 6.7% for NSP-BEA (30), NSP-BEA (50), and Si–Al–O, respectively. However, the C-BEA catalyst showed the greatest decrease in the reaction rate [207 mmol/(g-cat h) at 30 min to 143.2 mmol/(g-cat h); at 1 h, a 31.0% decrease in the reaction rate]. Fig. 4 also shows the regression curve (dashed line) for NSP-BEA (30), NSP-BEA (50), and Si–Al–O at a reaction time of 1 h. The relationship between the PX production rate and the amount of BA_{tot} on the catalysts still preserved the linearity. However, the C-BEA catalyst differed; it is marked by the dot (green colour triangle), which is far from this linear regression curve at a reaction time of 1 h. From the ICP-AES elemental analysis, the SiO_2/Al_2O_3 ratio for NSP-BEA (30) (SiO_2/Al_2O_3 = 31 in Table 1) does not much differ greatly from that of the C-BEA catalyst (SiO_2/Al_2O_3 = 26). While the total acidity (TA) and BA_{tot} for C-BEA (TA = 1144 μmol/g, BA_{tot} = 684 μmol/g) are greater than these for NSP-BEA (30) (TA = 820 μmol/g, BA_{tot} = 583 μmol/g), the DA cycloaddition/dehydration of DMF and ethylene with NSP-BEA (30) for the production of PX is more active than that of the C-BEA catalyst with a reaction time of 1 h. The catalytic result in C-BEA indicates that the zeolite structure, having only micropores, could lead to a large drop of the PX production rate at a reaction time of 1 h. It means that the micropores in C-BEA could be easily blocked by coke formation at the initial reaction time, after which then the catalytic activity could be lost because the reactants did not reach the active sites (Brønsted acid sites) in the micropores. The mesoporous-microporous structure of the NSP-BEA zeolites still maintained high catalytic activity in multi-phase reaction of DMF and ethylene to PX during the reaction. Because the main reason of catalytic deactivation is coking during PX production from DMF and ethylene, the existence of mesopores and external Brønsted acid sites in the NSP-BEA catalysts can reasonably explain the facile diffusion of reactants and products through the mesopores in the NSP-BEA zeolite as well as by the large number of Brønsted acid sites on the external mesopore surfaces, which could enhance the accessibility of the reactants to catalytic active site, and preserve the catalytic activity against the formation of heavy compounds as sources of coke. Similar phenomena were reported for various catalytic reactions in hierarchical zeolites [41,48,49]. We propose that this explains why the generation of mesopores in zeolite crystals can result in such high catalytic activity without significant deactivation. Therefore, the NSP-BEA zeolite having both micro-

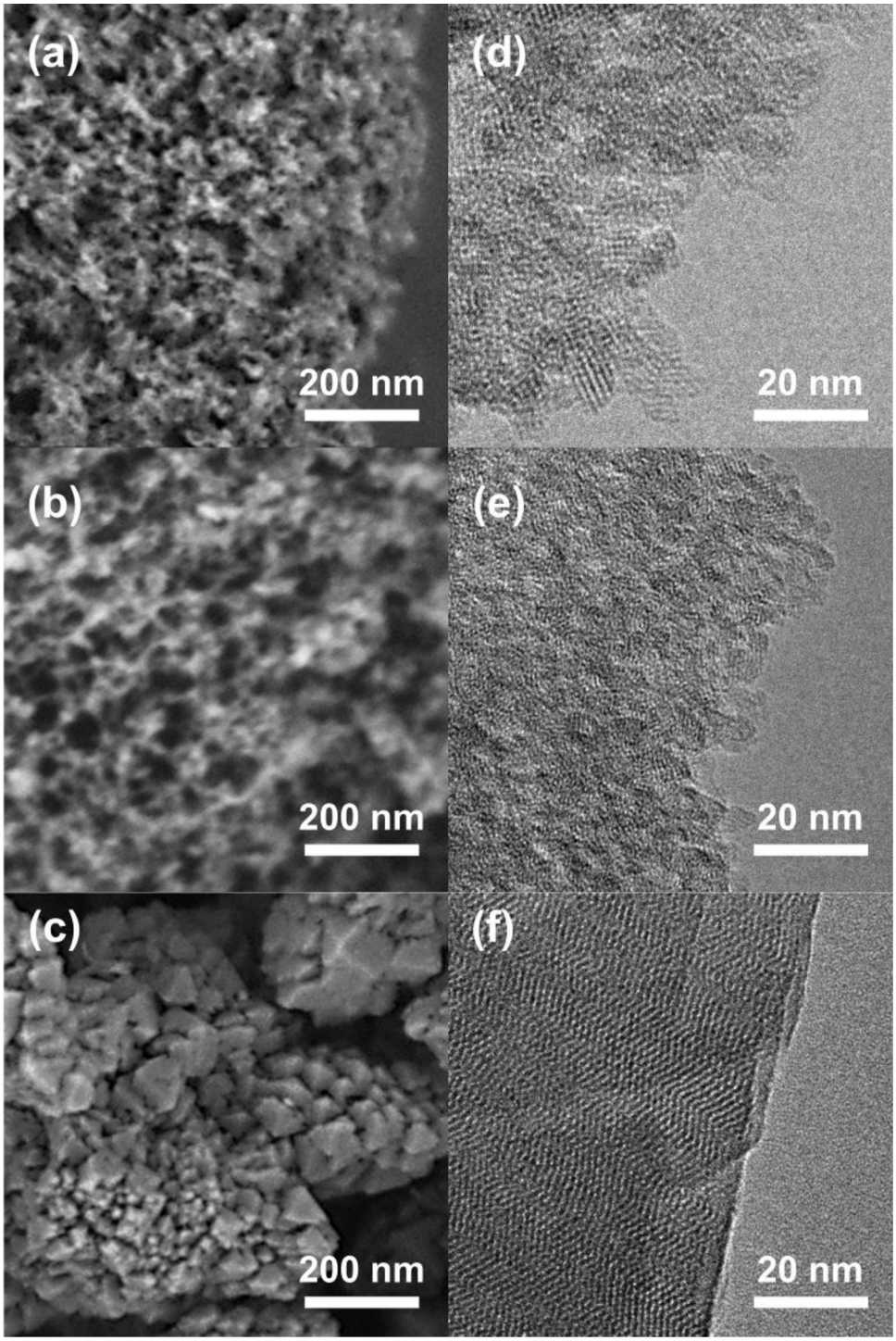

Fig. 2. SEM and TEM images of NSP-BEA (30) (a, d), NSP-BEA (50) (b, e) and C-BEA (c, f).

and mesoporosity is a more coke-tolerable catalyst compared with conventional beta zeolite. The turnover frequencies for the production of PX with catalysts were calculated by normalizing the rate by the number of Brønsted acid sites (H-TOF in Table 1). At the initial reaction time of 30 min, the value of H-TOF in the C-BEA catalyst is similar to that of NSP-BEA (30). This indicates that the two catalytic activity levels per Brønsted acid site in C-BEA and NSP-BEA (30) are nearly identical at 30 min. However, the value of H-TOF in C-BEA decreased greatly from the reaction time of 30 min to 1 h, while that of NSP-BEA (30) only decreased slightly. This provides another clue, showing that the formation of coke blocks micropores in C-BEA and then decreases the catalytic activity of the Brønsted acid sites on the surfaces of the micropores. For NSP-BEA (30), the decrease in the catalytic activity by coking in the micropores would be less affected due to the existence of a large amount of external Brønsted acid sites (BA_{ext} in Table 1) compared to the C-BEA catalyst.

Fig. 5 shows the conversion of DMF and the yields of PX and 2,5-hexanedione (HDO) as a function of the reaction time over various solid-acid catalysts up to 24 h. The beta zeolites and Si–Al–O catalysts show high DMF conversions which exceed 95% and PX yields greater than 60% after 24 h (Table 2). The conversion of the

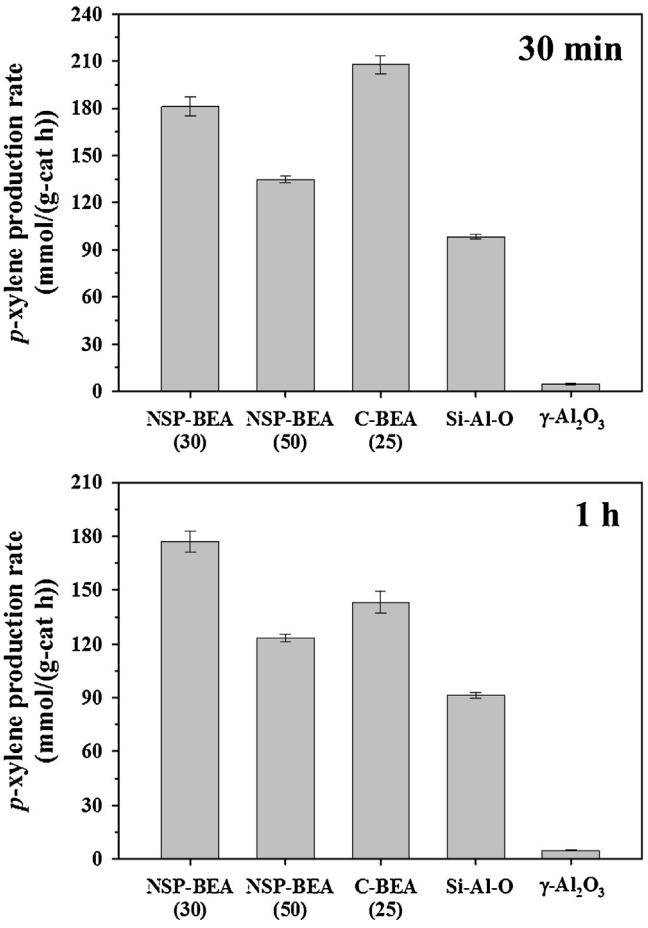

Fig. 3. Reaction rates of PX formation from DMF with ethylene (50 bar) at 250 °C with different catalysts and reaction times [30 min (up) and 1 h (bottom)]. The values in parentheses are SiO_2/Al_2O_3 ratios of the zeolites.

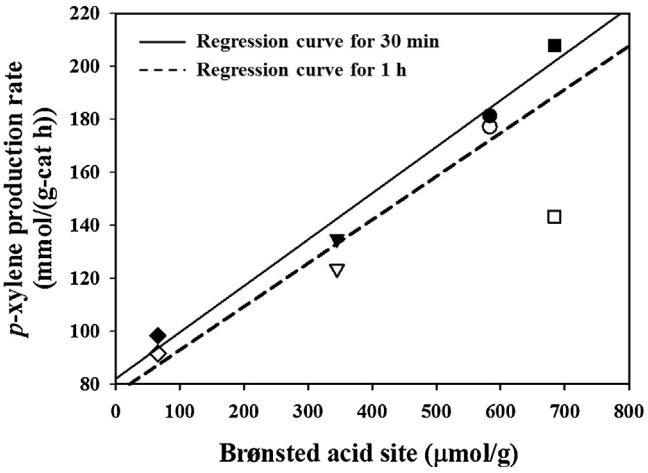

Fig. 4. Plot for total Brønsted acid site *versus* rate of PX production. The symbols and the colors represent the data at 30 min (closed symbol) and 1 h (open symbol) for NSP-BEA (30) (circle), NSP-BEA (50) (triangle), C-BEA (square), and Si–Al–O (diamond).

NSP-BEA (30) catalyst rapidly exceeded 80% within 3 h while the other solid catalysts having Brønsted acid sites took longer (~9 h) to obtain the same DMF conversion. However, γ-Al_2O_3 only exhibits a DMF conversion of approximately 40% and a PX yield close to 10% after 24 h, with a significant loss of its catalytic activity after 6 h. The lowest DMF conversion and PX yield of γ-Al_2O_3 in the long-term catalytic test reveal that the lack of Brønsted acid sites in the solid-acid catalyst leads to low catalytic activity with low PX selectivity. During the reaction time between 1 and 2 h, the PX yield of the NSP-BEA (30) catalyst was similar to that of the C-BEA catalyst, while the DMF conversion of NSP-BEA (30) was larger than that of C-BEA. This suggests that the PX selectivity in the NSP-BEA (30) catalyst was lower compared with the C-BEA catalyst. As shown in Fig. 5(c), the yield of HDO increased rapidly and decreased slowly in the NSP-BEA and Si–Al–O catalysts, with both having Brønsted acid sites and relatively large external surfaces compared with C-BEA. The NSP-BEA (30) catalyst reached the highest HDO yield with the shortest reaction time, showing the lowest HDO yield after 5 h, except for the γ-Al_2O_3 catalyst. However, the C-BEA catalyst showed an increase in the HDO yield up to 12 h and then a small decrease in the HDO yield. According to the reaction pathway of the production of PX from DMF and ethylene, shown in Fig. S3 [30,31], HDO is produced by means of DMF hydrolysis with water from the dehydration of the cycloadduct intermediate; this hydrolysis reaction is a reversible reaction to maintain equilibrium between the DMF and HDO [50]. Assuming that the NSP-BEA (30) and C-BEA catalysts both have good catalytic activity and a sufficient amount of Brønsted acid sites for PX production from DMF and ethylene, the micro- and mesoporous structure with a large amount of external acid sites in the NSP-BEA (30) catalyst would quickly produce PX and water from DMF and ethylene due to the consecutive DA cycloaddition and dehydration processes. The water produced would sharply increase the HDO yield by DMF hydrolysis during the initial reaction time (~1 h). As DMF is rapidly converted to PX over the NSP-BEA (30) catalyst during the reaction time due to the existence of mesopores with a large amount of external Brønsted acid sites, the HDO is readily converted to DMF to maintain the equilibrium between the DMF-H_2O and the HDO [32]. However, the C-BEA catalyst, having only micropores, showed a gradual increase in the HDO yield up to 12 h and a small decrease over the next 12 h due to the blocking of active sites in the micropores by coke formation.

The spent NSP-BEA (30), and C-BEA catalysts were extensively washed with iso-propyl alcohol and dried at 100 °C for the preparation of TGA analyses to determine coke depositions in the catalysts with time. As shown in Fig. S4, both catalysts show that most of coke was deposited during the initial period, and the amount of coke for NSP-BEA (30) catalyst was smaller than that of C-BEA overall reaction period. From these results, it would indicate that most coke was formed on active sites in micropores during the initial reaction time by using a batch reactor, and NSP-BEA (30) catalyst is more coke-tolerable than C-BEA as discussed above.

In Fig. S5 and S6, a series of fresh, washed, and calcined both NSP-BEA (30) and C-BEA samples were analysed by XRD and nitrogen sorption. After the reaction (in 24 h), the spent catalysts were recovered, and extensively washed with iso-propyl alcohol (denoted as washed-NSP-BEA (30) and washed-C-BEA). The samples were subsequently calcined at 550 °C (denoted as calcined-NSP-BEA (30) and calcined-C-BEA). The XRD pattern and N_2 isotherm of calcined-NSP-BEA (30) sample are similar to pristine-NSP-BEA sample. The lower intensity of XRD peak around 7.5°, and small surface area and pore volume for washed-NSP-BEA (30) compared with fresh- and calcined-samples was due to the coke deposition of the catalyst during the reaction. The shoulder peak of calcined-NSP-BEA (30) around 1.5° in the low-angle XRD pattern was still preserved, which indicates that NSP-BEA (30) catalyst maintained its mesoporosity after the reaction. From these results we conclude that, NSP-BEA catalyst has a structurally good stability under the reaction conditions. The XRD and N_2 isotherm for calcined-C-BEA sample are also similar to pristine-C-BEA. It implies that the reaction condition did not affect the structure of C-BEA.

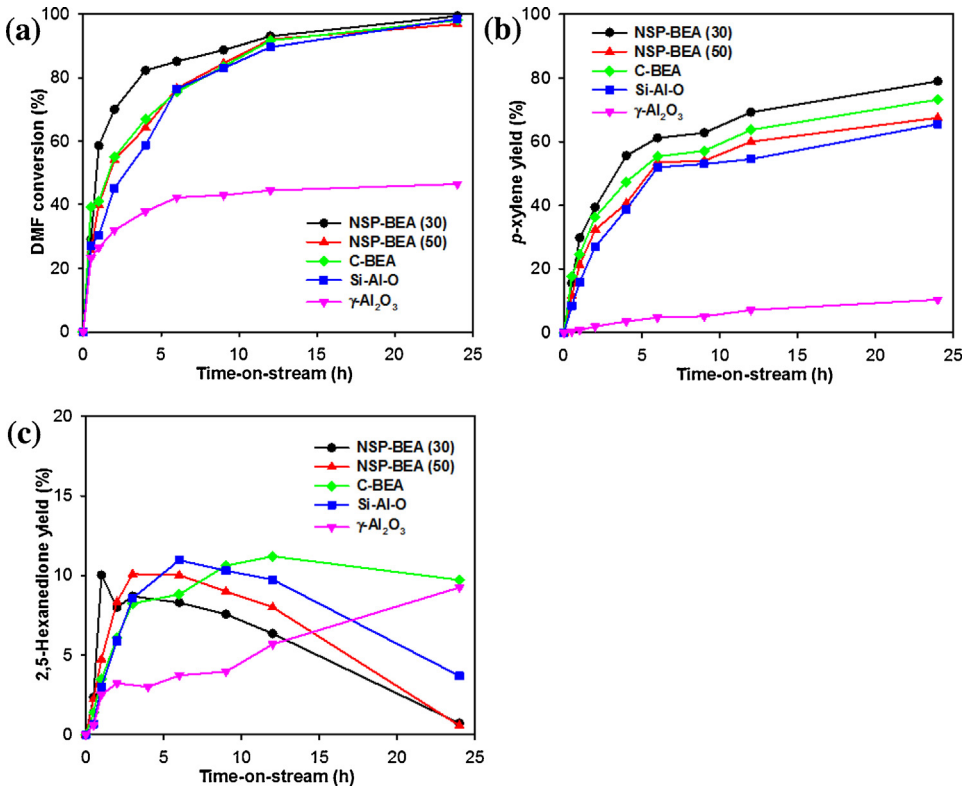

Fig. 5. (a) DMF conversion, (b) PX yield, and (c) 2, 5-hexanedione yield as a function of time under 50 bar of ethylene at 250 °C with different catalysts.

Table 2
Catalytic activities of various catalysts for the *p*-xylene production from DMF with ethylene (50 bar) at 250 °C, 24 h.

Catalyst	DMF conv. (%)[a]	PX yield (%)	Selectivity (mol%)			
			PX	MX	HDO	Unknown products
NSP-BEA (30)	99.3	79.4	80.0	4.5	0.7	14.8
NSP-BEA (50)	97.7	67.5	69.7	5.6	0.6	24.1
C-BEA	98.0	73.2	74.7	–	9.9	15.4
Si-Al-O	98.4	65.5	66.6	2.4	3.8	27.2
γ-Al_2O_3	46.5	10.4	22.3	–	19.9	57.8

[a] DMF conv., DMF conversion; PX yield, *p*-xylene yield; PX, *p*-xylene; MX, *m*-xylene; HDO, 2,5-hexanedione; Unknown products, carbon loss.

3.3. *Effect of the NSP-BEA catalyst with different reaction conditions*

In order to determine the reaction conditions for a high yield of PX, the optimum catalyst, NSP-BEA (30), was applied in the DA cycloaddition/dehydration of DMF and ethylene with different reaction conditions, in this case different reaction temperatures, pressures, masses of the catalyst, and DMF/solvent ratios. As shown in Fig. 6(a), the NSP-BEA catalyst was tested with various temperatures ranging from 225 to 300 °C (other reaction conditions: 0.2 g catalyst, 50 bar, and 25 vol% DMF in *n*-heptane). The best catalytic performance occurred at 250 °C, which exhibited the highest DMF conversion and PX selectivity with the lowest selectivity of unknown products as byproducts. In the lower temperature range (225–250 °C), the PX yield increases with an increase in the temperature. It is due to that higher temperature facilitates the dehydration of the cycloadduct intermediate (1,4-dimethyl-7-oxabicyclo[2.2.1]hept-2-ene) and because the conversion rate of the cycloadduct intermediate to PX is higher than the decreasing rate of the feed stocks [36]. At temperatures exceeding 250 °C, DMF conversion and PX and HDO selectivities of the NSP-BEA (30) catalyst decreased as the reaction temperature increased, whereas the unknown products increased largely. The increase in the unknown products at temperatures which exceeded 250 °C indicates that HDO and PX could be further converted to byproducts such as oligomers and alkylated compounds via the oligomerization of HDO and the alkylation of aromatics.

Fig. 6(b) shows the catalytic activity of the NSP-BEA (30) catalyst at various pressures ranging from 30 to 60 bar (0.2 g catalyst, 250 °C, 25 vol% DMF in *n*-heptane). An increase in the reactor pressure from 30 to 50 bar gradually increases both the conversion of DMF and the selectivity of PX and reduces the amount of unknown products. At the highest pressure (60 bar), the DMF conversion is similar to that at 50 bar, but the selectivity of PX decreases due to the increase in the selectivity of the unknown products. The batch-type reactor was pressurized with ethylene gas. Thus, an increase in the reaction pressure caused an increase in the partial pressure of ethylene gas; this should directly affect the DA cycloaddition of DMF and ethylene to form the cycloadduct intermediate as depicted in Fig. S3. The DA cycloaddition is a reversible reaction that maintains the state of equilibrium between DMF-ethylene and cycloadduct intermediate, and the cycloadduct intermediate readily converts to PX by dehydration in the presence of a Brønsted acid-catalyst. From the computed free energy barriers of the DMF/ethylene cycloaddition and cycloadduct intermediate dehydration, the rate-determining step over a solid-acid catalyst having Brønsted acid sites is the

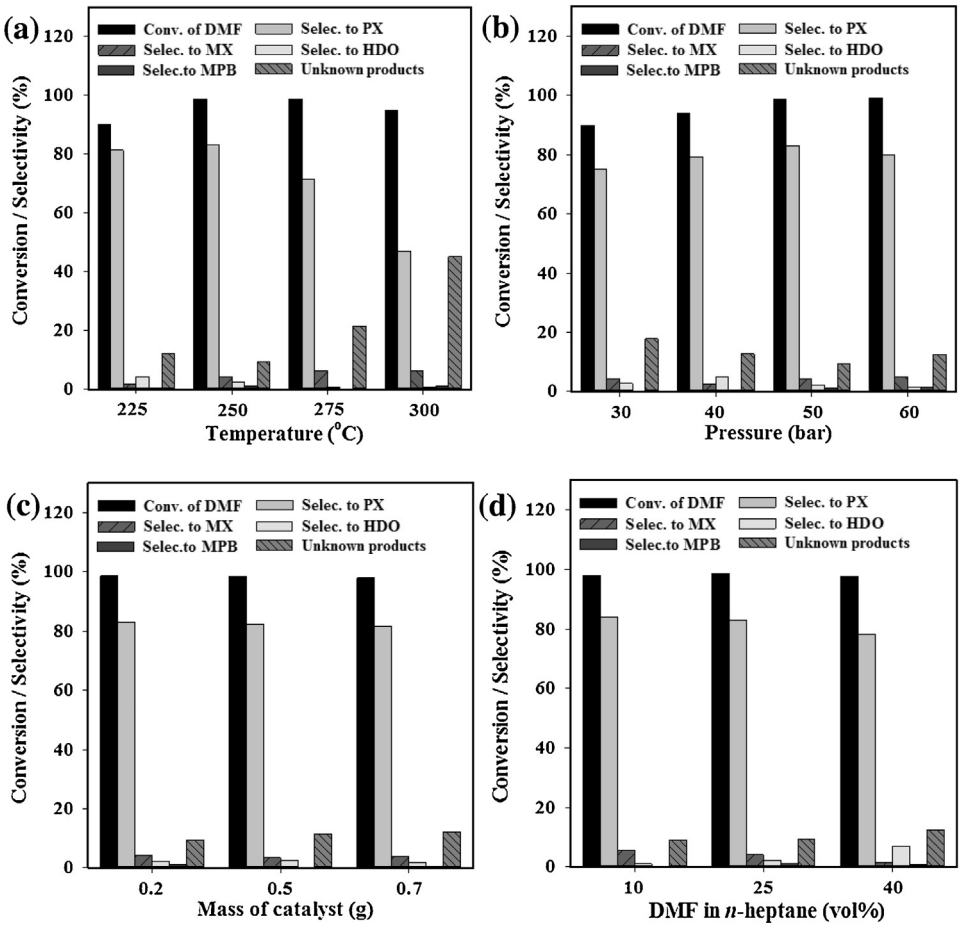

Fig. 6. DMF conversions and product selectivities of NSP-BEA (30) catalyst with different reaction (a) temperature, (b) pressure, (c) amount of catalyst, and (d) amount of DMF in *n*-heptane.

formation of one cycloadduct intermediate molecule from two feed molecules (DMF and ethylene) via DA cycloaddition [28]. This means that the energy barrier of the formation of a bicyclic intermediate is higher that of the production of PX via the dehydration of the intermediate and that the DA cycloaddition reaction is thermodynamically unfavorable compared with the dehydration reaction over the Brønsted acid-catalyst. Therefore, an increase in the reaction pressure, which caused by the partial pressure of ethylene gas, would increase both the DMF conversion and PX selectivity up to a reaction pressure of 50 bar.

The effects of the catalyst amount were investigated using different quantities of catalyst from 0.2 to 0.7 g at 250 °C, 50 bar, and 25 vol% DMF in *n*-heptane. As shown in Fig. 6(c), the DMF conversion and product selectivities were slightly changed with different amounts of catalyst. This finding indicates that the catalyst amount does not have a great effect on the catalytic activity during PX production when using a batch-type reactor for 24 h. The ratio of DMF and *n*-heptane as a solvent was tested with different DMF volumes in *n*-heptane ranging from 10 to 40 vol% (0.2 g catalyst, 250 °C, 50 bar). *n*-Heptane is reportedly a good and inert aliphatic solvent during the production PX from DMF and ethylene due to the suppressed formation of unknown products [28]. In Fig. 6(d), with an increase in the DMF amount (also with a decrease in the amount of *n*-heptane), the conversion of DMF remained nearly unchanged, but the xylene selectivities gradually decreased with an increase in the selectivities of HDO and unknown products. The catalytic result could be explained by recent computational studies which showed that the introduction of *n*-heptane results in a lower probability of the formation of unknown products due to a decrease in the loading of DMF in a zeolite catalyst [50]; this reduces side reactions with water through less water adsorption in a zeolite catalyst due to an increase of the hydrophobic environment in the zeolite catalyst [51].

4. Conclusion

The nanosponge beta (NSP-BEA) catalysts with large surface areas and a meso-micro hierarchical structure were synthesized as catalysts for production of PX from DMF and ethylene via consecutive reactions of Diels–Alder (DA) cycloaddition and dehydration. The NSP-BEA (30) catalyst exhibited the best catalytic performance among the C-BEA, γ-Al_2O_3, and Si–Al–O catalysts. Notably, except for the initial reaction time of 30 min, a higher DMF conversion and better PX selectivity were achieved with the NSP-BEA zeolite and were preserved during further reaction times compared with the C-BEA zeolite catalyst, which is known as an effective catalyst for DA cycloaddition among zeolites due to its micropores equipped with strong Brønsted acid sites. This better catalytic performance of the NSP-BEA catalysts could be attributed to mesopores and a large number of Brønsted acid sites on the external surfaces. The existence of mesopores with a large amount of external Brønsted acid sites facilitates the accessibility of the reactants to catalytic active sites while also making NSP-BEA a coke-tolerable catalyst.

Acknowledgments

The authors would like to acknowledge the funding from the R&D Convergence Program of MSIP (Ministry of Science, ICT and

Future Planning) and ISTK (Korea Research Council for Industrial Science and Technology) of the Republic of Korea (Grant 13-6-KIER). This work was supported by IBS-R004-D1.

Appendix A. Supplementary data

Supplementary data associated with this article can be found, in the online version, at http://dx.doi.org/10.1016/j.apcatb.2015.11.046.

References

[1] W. Partenheimer, Catal. Today 23 (1995) 69–158.
[2] D.I. Collias, A.M. Harris, V. Nagpal, I.W. Cottrell, M.W. Schultheis, Ind. Biotechnol. 10 (2014) 91–105.
[3] H.A. Wittcoff, B.G. Reuben, J.S. Plotkin, Industrial Organic Chemicals, John Wiley & Sons, Inc., 2005, http://dx.doi.org/10.1002/0471651540 (chapter 9).
[4] R.A. Sheldon, Green Chem. 16 (2014) 950–963.
[5] UOP, Capturing Opportunities for Para-xylene Production, http://www.uop.com/?document=uop-capturing-opportunities-for-para-xylene-production-tech-paper&download=1, Accessed (12.08.14.).
[6] PCI, Paraxylene & Derivatives World Supply & Demand Report 2012, 2012.
[7] G. Qu, Opportunities and Developments in para-Xylene Production, http://www.uop.com/wp-content/uploads/2012/12/Opportunities-and-Developments-in-pX-Production_China-pX-DevelopmentForum_April-2014pdf, accessed (13.08.14.).
[8] J.A. Posada, A.D. Patel, A. Roes, K. Blok, A.P.C. Faaij, M.K. Patel, Bioresour. Technol. 135 (2013) 490–499.
[9] P.C.A. Bruijnincx, B.M. Weckhuysen, Angew. Chem. Int. Ed. 52 (2013) 11980–11987.
[10] M.J. Climent, A. Corma, S. Iborra, Green Chem. 13 (2011) 520–540.
[11] J. Fabri, U. Graeser, T.A. Simo, Ullmann's Encyclopedia of Industrial Chemistry, Wiley-VCHVerlag GmbH & Co. KGaA, 2000, 2015, http://dx.doi.org/10.1002/14356007.a28_433.
[12] J. Speight, Chemical Process and Design Handbook, McGraw-Hill Education, New York, 2001.
[13] Y.Y. Fong, A.Z. Abdullah, A.L. Ahmad, S. Bhatia, Chem. Eng. J. 139 (2008) 172–193.
[14] T.-C. Tsai, S.-B. Liu, I. Wang, Appl. Catal. A: Gen. 181 (1999) 355–398.
[15] P. Lu, Z. Fei, L. Li, X. Feng, W. Ji, W. Ding, Y. Chen, W. Yang, Z. Xie, Appl. Catal. A: Gen. 453 (2013) 302–309.
[16] W. Alabi, L. Atanda, R. Jermy, S. Al-Khattaf, Chem. Eng. J. 195–196 (2012) 276–288.
[17] Z. Zhu, Q. Chen, W. Zhu, D. Kong, C. Li, Catal. Today 93–95 (2004) 321–325.
[18] B. Xue, J. Su, Q. Huang, J. Xu, Y. Li, Catal. Commun. 45 (2014) 49–53.
[19] B. Xue, Y. Li, L. Deng, Catal. Commun. 10 (2009) 1609–1614.
[20] M. Ghiaci, A. Abbaspur, M. Arshadi, B. Aghabarari, Appl. Catal. A: Gen. 316 (2007) 32–46.
[21] E. de Jong, A. Higson, P. Walsh, M. Wellisch, Biofuels Bioprod. Biorefin. 6 (2012) 606–624.
[22] United States Patent., 8455705, 2013.
[23] Virent, Bio-based PX for 100% bio-PET, http://www.virent.com/wordpress/wp-content/uploads/2013/12/Presentation-at-Ecochem-International-Conference-on-Sustainable-Chemistry-and-Engineering.pdf, Accessed (12.08.14.).
[24] Anellotech, Simple, novel technology for producing 'clean' petrochemicals and transportation fuels, http://anellotech.com/tech.html, Accessed (08.08.14.).
[25] US Patent., US20130324772 A1, 2013.
[26] Gevo, Isobutanol, http://www.gevo.com/, Accessed (08.07.14.).
[27] US Patent., US20110087000 A1, 2011.
[28] C.L. Williams, C.-C. Chang, P. Do, N. Nikbin, S. Caratzoulas, D.G. Vlachos, R.F. Lobo, W. Fan, P.J. Dauenhauer, ACS Catal. 2 (2012) 935–939.
[29] US Patent., US 8314267 B2, 2009.
[30] N. Nikbin, P.T. Do, S. Caratzoulas, R.F. Lobo, P.J. Dauenhauer, D.G. Vlachos, J. Catal. 297 (2013) 35–43.
[31] P.T.M. Do, J.R. McAtee, D.A. Watson, R.F. Lobo, ACS Catal. 3 (2013) 41–46.
[32] C.-C. Chang, S.K. Green, C.L. Williams, P.J. Dauenhauer, W. Fan, Green Chem. 16 (2014) 585–588.
[33] JP Patent., WO2009110402 A1, 2009.
[34] J.J. Bozell, G.R. Petersen, Green Chem. 12 (2010) 539–554.
[35] Y. Roman-Leshkov, C.J. Barrett, Z.Y. Liu, J.A. Dumesic, Nature 447 (2007) 982–985.
[36] D. Wang, C.M. Osmundsen, E. Taarning, J.A. Dumesic, ChemCatChem 5 (2013) 2044–2050.
[37] M. Choi, K. Na, J. Kim, Y. Sakamoto, O. Terasaki, R. Ryoo, Nature 461 (2009) 246–249.
[38] W. Kim, J.-C. Kim, J. Kim, Y. Seo, R. Ryoo, ACS Catal. 3 (2013) 192–195.
[39] Y. Seo, K. Cho, Y. Jung, R. Ryoo, ACS Catal. 3 (2013) 713–720.
[40] C. Jo, J. Jung, R. Ryoo, Micropor. Mesopor. Mater. 194 (2014) 83–89.
[41] J.-C. Kim, K. Cho, R. Ryoo, Appl. Catal. A: Gen. 470 (2014) 420–426.
[42] M.V. Opanasenko, M.V. Shamzhy, C. Jo, R. Ryoo, J. Čejka, ChemCatChem 6 (2014) 1919–1927.
[43] E. Verheyen, C. Jo, M. Kurttepeli, G. Vanbutsele, E. Gobechiya, T.I. Korányi, S. Bals, G. Van Tendeloo, R. Ryoo, C.E.A. Kirschhock, J.A. Martens, J. Catal. 300 (2013) 70–80.
[44] K. Na, M. Choi, R. Ryoo, Micropor. Mesopor. Mater. 166 (2013) 3–19.
[45] K. Na, C. Jo, J. Kim, K. Cho, J. Jung, Y. Seo, R.J. Messinger, B.F. Chmelka, R. Ryoo, Science 333 (2011) 328–332.
[46] J.H. Lunsford, W.P. Rothwell, W. Shen, J. Am. Chem. Soc. 107 (1985) 1540–1547.
[47] K. Cho, K. Na, J. Kim, O. Terasaki, R. Ryoo, Chem. Mater. 24 (2012) 2733–2738.
[48] J.-C. Kim, R. Ryoo, M.V. Opanasenko, M.V. Shamzhy, J. Čejka, ACS Catal. 5 (2015) 2596–2604.
[49] J.-C. Kim, K. Cho, S. Lee, R. Ryoo, Catal. Today 243 (2015) 103–108.
[50] Y.-P. Li, M. Head-Gordon, A.T. Bell, J. Phys. Chem. C 118 (2014) 22090–22095.
[51] R. Xiong, S.I. Sandler, D.G. Vlachos, P.J. Dauenhauer, Green Chem. 16 (2014) 4086–4091.